Lithium intercalation into TiO_2(B): A comparison of LDA, GGA, and GGA + U density functional calculations

Benjamin J. Morgan* and Paul A. Madden
Department of Materials, University of Oxford, Parks Road, OX1 3PH, United Kingdom
(Received 22 May 2012; published 27 July 2012)

Density functional theory has been used to study lithium intercalation into TiO_2(B) at low to moderate concentrations [$0 < x(\mathrm{Li}) \leqslant 0.25$] with a range of density functionals: LDA, GGA (PW91, PBE, PBEsol), and GGA + U (PBE + U, PBEsol + U), with the GGA + U calculations employing a Hubbard + U correction to the Ti d states. LDA and GGA functionals give the same general behavior, whereas qualitatively different behavior is predicted by GGA + U for electronic structure and the order of stability of occupied intercalation sites. LDA/GGA functionals predict Li_xTiO_2(B) to be metallic, with the excess charge distributed over all the Ti sites. In contrast, GGA + U predicts defect states in the band gap corresponding to charge strongly localized at specific Ti sites. All the considered functionals predict A1 and/or A2 site occupation at $x(\mathrm{Li}) = 0.25$, which challenges the interpretation of previous neutron data that, at this composition, the C site is preferentially occupied.

DOI: 10.1103/PhysRevB.86.035147 PACS number(s): 82.47.Aa, 71.20.Tx

I. INTRODUCTION

Titanates have been proposed as alternatives to conventional graphite anodes in lithium-ion batteries,[1–3] for use in portable electronics, and large-scale applications such as hybrid electric vehicles. The electrochemical potential of graphite anodes lies above the lowest unoccupied orbitals of typical Li battery electrolytes, rendering these susceptible to reduction unless an insulating solid/electrolyte-interface (SEI) layer is present.[4] The formation of the SEI layer involves an irreversible capacity loss, and places limitations on cell charge/discharge rates: fast charging can cause Li^+ accumulation and disruption of the SEI layer, allowing outgrowth of Li dendrimers and potentially resulting in catastrophic short circuiting of the cell. TiO_2 readily intercalates lithium, and as an anode material demonstrates an electrochemical potential below the lowest unoccupied molecular orbital (LUMO) of typical electrolytes, removing the requirement for a SEI layer.[4] Consequently, cell safety and charge/discharge rates are expected to be improved over cells utilizing graphite anodes. The lower electrochemical potential of lithiated TiO_2 relative to graphite results in decreased cell voltage and total energy capacity. This voltage reduction is offset for TiO_2(B), which can store a greater total amount of intercalated lithium than the more common anatase and rutile phases.[1,5,6] Additional improvements in performance have been demonstrated for nanocrystalline and nanotubular TiO_2(B), which are able to accommodate increased amounts of intercalated lithium, and where the reduction in typical diffusion lengths leads to increased charge/discharge rates and power output.[7–10]

The TiO_2(B) structure is constructed from edge- and corner-sharing TiO_6 octahedra, and has three crystallographically distinct sites available to accommodate intercalated lithium, denoted A1, A2, and C (Fig. 1).[11] The C sites are arranged in infinite channels aligned along b, which facilitate diffusion of lithium along this axis.[12,13] Offset from each C site along $\pm a$ and $\pm c$, respectively, are pairs of A1 and A2 sites, which both have square-pyramidal fivefold coordination. The C sites are larger than the A1 and A2 sites, and Li is thought to occupy an off-center position with a small displacement along b, giving a [2 + 2] coordination, where these four ions lie in a (010) plane away from the interstice center.[10,12,14]

Understanding how intercalated lithium is distributed amongst these available sites is fundamental to explaining the electrochemical behavior of TiO_2(B) anodes. Intercalation energies at each site determine electrode potentials, and specific features in experimental differential capacity plots have been interpreted as changes in site preference as a function of Li content.[10] In addition, competition between the lowest-energy site and metastable alternatives has been proposed to contribute towards the initial capacity loss seen in experimental samples, and to possibly cause pseudocapacitive rather than diffusion-limited intercalation of Li.[3,13,15]

Armstrong *et al*. have reported powder neutron diffraction data for Li_xTiO_2(B) across a range of lithium concentrations. For a stoichiometry of $Li_{0.15}TiO_2$(B), they were unable to satisfactorily index the neutron data to a single phase, but instead identified a phase-separated mixture of TiO_2(B) and $Li_{0.25}TiO_2$(B). For this low-Li regime, where the Li is concentrated in $Li_{0.25}TiO_2$ regions, the C site was identified as being preferentially occupied, with the lithium sitting in an off-center position displaced 0.63 Å along b.[10]

The preference for lithium to occupy specific sites in TiO_2(B) has previously been investigated with density functional theory (DFT) calculations by Panduwinata and Gale, by Arrouvel *et al*., and by Dalton *et al*.[12–14] Each of these studies, however, has suggested a different preferred interstitial site at low-Li content. Panduwinata and Gale reported Perdew-Burke-Ernzerhof (PBE) [generalized gradient approximation (GGA)] calculations for $x(\mathrm{Li}) \approx 0.02$ that predicted that the A2 site is favored, with relative site occupation energies [$E(\mathrm{A2}) < E(\mathrm{C}) < E(\mathrm{A1})$] of [$0 < 0.094 < 0.336$] eV. Compositions up to $x(\mathrm{Li}) = 0.5$ were also considered, and at $x(\mathrm{Li}) \geqslant 0.125$, lithium was found to be preferentially distributed over the A2 and A1 sites, although no geometries or relative energies for specific configurations were presented. This result then contradicts the experimental data of Armstrong *et al*., which indicate that at a composition of $x(\mathrm{Li}) = 0.25$ the C sites are occupied.[10]

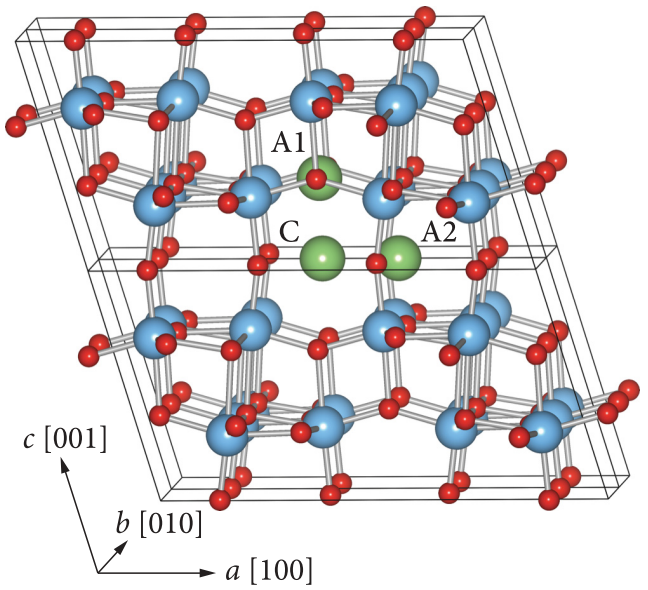

FIG. 1. (Color online) The three sites available for Li intercalation in TiO_2(B). Titanium ions are shown in blue, oxide ions in red, and lithium ions in green.

Arrouvel *et al.* performed PW91 (GGA) calculations for a composition of $x(\mathrm{Li}) = 0.125$,[12] and found that the C site was preferred, with relative site energies $[E(\mathrm{C}) < E(\mathrm{A2}) < E(\mathrm{A1})]$ of $[0.00 < 0.09 < 0.15]$, in apparent agreement with the neutron data of Armstrong *et al.*[10] and contrary to the calculations of Panduwinata and Gale.[13] Calculations performed at this lithium concentration may, however, be unrepresentative of experimental samples. The C-site assignment from experimental data can be attributed to the $x(\mathrm{Li}) = 0.25$ phase, which may exhibit different Li-Li interactions and site energies to a homogeneous phase with a composition of $x(\mathrm{Li}) = 0.125$. Furthermore, these calculations were performed with a unit-cell shape constrained to be equal to that of stoichiometric TiO_2(B).[12] Experimental data show there is a highly anisotropic change of cell shape between the TiO_2(B) and $Li_{0.25}TiO_2$(B) phases: +5.8%, +1.6%, and −0.3% along a, b, and c respectively;[10,12] and calculations performed with only an isotropic relaxation of volume (equivalent to an anisotropic pressure) may give different relative site energies than from a full geometric relaxation. Therefore, despite the apparent consistency with the experimental data, the consequences for the relative site energies of a different lithium content and constrained cell shape need to be taken into account.

Dalton *et al.* also considered a composition of $x(\mathrm{Li}) = 0.125$ using PBE (GGA) and reported relative site energies of $[E(\mathrm{A1}) < E(\mathrm{A2}) < E(\mathrm{C})]$ of $[0.00 < 0.032 < 113]$, with the same trend at a composition of $x(\mathrm{Li}) = 0.25$. These data then disagree with the neutron data and with the studies of Panduwinata and Gale and Arrouvel *et al.*[12,13] Despite the use of highly similar theoretical methods then, each of these three studies has led to a different prediction of the favored Li site at these low-Li compositions.

A further factor not considered in previous DFT studies of Li_xTiO_2(B) is the ability of standard functionals (LDA/GGA) to accurately describe the electronic structure of this system. Electrochemical intercalation of lithium into TiO_2 can be represented as

$$TiO_2 + xLi^+ + xe^- \rightarrow Li_xTiO_2, \quad (1)$$

where x is the mole fraction of lithium. For the related anatase Li-TiO_2 system, experimental photoemission spectra show that as lithium is progressively intercalated, a feature appears in the band gap with a binding energy of ∼1.0 eV. This gap state is attributed to occupied Ti 3d states, with core x-ray photoemission spectroscopy (XPS) and resonant inelastic soft x-ray scattering also indicating the presence of Ti^{3+} species.[16–19] Similar gap-state features have been observed for a number of reduced or n-type doped TiO_2 systems.[20–22] In the case of O-deficient rutile TiO_2, electron paramagnetic resonance data show that the excess electrons are strongly localized at titanium sites near the vacancy,[23,24] with similar localization reported for fluorine-doped rutile TiO_2.[25] Polaronic localization of charge may not occur for all reduced/n-type TiO_2 systems, however, with specific behavior depending on the particular TiO_2 phase and the source of excess electrons. For example, fluorine- and niobium-doped anatase TiO_2 are thought to exhibit Ti^{3+} states that are less strongly localized than in the rutile analogs.[26–29]

For n-type TiO_2 systems where experiment indicates the existence of polaronic Ti^{3+} defect states, as for lithium-intercalated anatase-TiO_2, standard density functionals (LDA/GGA) fail to even qualitatively describe the electronic structure.[30–36] Instead, such calculations predict that the bottom of the conduction band is occupied, corresponding to a metallic system with excess charge distributed over all available Ti centers. This is a consequence of the self-interaction error inherent to standard functionals,[37–39] and which is acute for highly localized transition-metal and rare-earth d and f states. Erroneous delocalization of defect states in contradiction with experimental evidence has been shown to be a problem for a large number of systems when modeled with standard density functionals.[40–51]

One approach to correcting this deficiency due to the self-interaction error is to apply a "+U" term to the states of interest, where the onsite Coulomb interaction within the chosen functional is replaced with a Hubbard term.[52,53] This gives improved descriptions of polaronic defect states in a number of oxides, including lithium-intercalated systems.[33,34,36,45,49,54–67] In the case of Li-intercalated anatase TiO_2, GGA + U calculations successfully predict a defect state ∼1.0 eV below the conduction band, in agreement with the experimental XPS data, with this state corresponding to charge localized as a small polaron at a Ti center neighboring the Li intercalation site.[36] In addition to recovering qualitative agreement with experimental data, correcting for the self-interaction error has also been shown to typically improve redox potentials, with Zhou *et al.* reporting an order-of-magnitude improvement in accuracy between GGA and GGA + U calculations for a number of transition-metal compounds.[68]

Panduwinata and Gale have argued that energetic trends are typically unchanged by the addition of a +U term, and so relative site energies in TiO_2(B) can be expected to follow the same behavior between, e.g., PBE and PBE + U data.[13] This assertion has not been tested, however, and is

challenged by the work of Arrouvel *et al.* who reported that PW91 versus PW91 + U calculations, with a $U = 4$ eV applied to Ti d states, gave *different* orderings of the site energies.[12] The PW91 calculations predicted that the C site is favored at x(Li) = 0.125, in agreement with the experimental neutron data of Armstrong *et al.*[10] For PW91 + U, the C site was disfavored, and it was argued that this failure to agree with experimental data makes $+U$-corrected calculations a poor choice for modeling Li_xTiO_2(B). This change in site preference was attributed to the difference in equilibrium volumes between the PW91 and PW91 + U calculations. Both functionals overestimate volumes with respect to experiment, but this error is typically larger for $+U$-corrected functionals. Arrouvel *et al.* argued that this greater overestimation of the volume corresponds to the C site becoming too large to favorably accommodate intercalated lithium, instead favoring A1/A2 occupation.[10]

Here, we report density functional calculations of Li_xTiO_2(B) at x(Li) = 0.02,0.125,0.25 using LDA, GGA (PW91, PBE, PBEsol), and GGA + U (PBE + U and PBEsol + U). For each combination of Li composition and functional, we have calculated the relative energies for Li occupation of the A1, A2, or C sites. Performing calculations at these compositions across a range of functionals allows us to make direct comparisons with the data of Panduwinata and Gale [PBE, x(Li) = 0.02], Arrouvel *et al.* [PW91, x(Li) = 0.125], and Dalton *et al.* [PBE, x(Li) = 0.125], for which relative energies of the competing intercalation sites have previously been published.[12–14] We are also able to separately compare the effect of functional choice on predicted site stability across a range of low- to moderate-Li concentrations. This selection of functionals allows us to examine the relationship between equilibrium cell volumes and the relative energies of the Li intercalation sites: LDA typically underestimates cell volumes, while GGA (PW91, PBE) typically overestimates cell volumes. PBEsol is a revised PBE-GGA functional that offers improved equilibrium properties of solids relative to the standard PBE.[69] The $+U$ supplemented GGA functionals are expected to show even greater overestimations of cell volumes. It is also of interest to consider the consequences for electronic structure and cell voltage in employing a $+U$-corrected functional to model lithium intercalation into TiO_2(B). Li_xTiO_2(B) is expected to behave similarly to other better studied polytypes where addressing the self-interaction error has been shown to be necessary to reproduce features of the electronic structure consistent with experimental observations.[36] We also report sample calculations using the Heyd-Scuseria-Ernzerhof (HSE06) hybrid density functional, which offers an alternative methodology for accounting for the self-interaction error inherent to standard density functionals, and that avoids some of the empiricism of the GGA + U functionals, albeit at a much greater computational expense.

II. METHOD

Calculations were performed using the density functional theory code VASP,[70,71] with valence electrons described within a plane-wave basis and a cutoff of 500 eV. Valence-core interactions were treated with the projector augmented wave (PAW) method,[72,73] with cores of [Ar] for Ti, [He] for O, and [He] for Li. We have performed calculations using the LDA,[74] and PW91, PBE, and PBEsol GGA functionals.[69,75,76] PBE and PBEsol calculations supplemented with a Dudarev $+U$ correction of $U = 4.2$ eV applied to Ti d states (GGA + U) were also performed.[52] This U value was obtained by previously fitting to experimental data on the splitting between occupied and unoccupied Ti d states for oxygen vacancy states at the (110) surface of rutile,[31] and has been used to model oxygen vacancies at other rutile surfaces, Nb and Ta substitution, and native defect formation in rutile and anatase,[34,63,64] as well as lithium intercalation into anatase.[36]

Calculations for stoichiometric TiO_2(B) and Li_xTiO_2(B) for $x = 0.125,0.25$ were performed for single unit cells, with Γ-centered $3 \times 7 \times 5$ Monkhorst-Pack k-point meshes. Calculations for Li_xTiO_2(B) at $x \approx 0.02$ were performed for a $1 \times 3 \times 2$ supercell using a $3 \times 3 \times 3$ Γ-centered Monkhorst-Pack k-point grid. All calculations where lithium was included were spin polarized, and for x(Li) = 0.25, where two excess electrons are present, "singlet" ($M_S = 0$) and "triplet" ($M_S = 1$) spin states were explicitly compared. Full geometry optimizations were performed, with zero-pressure volumes obtained by performing a series of constant volume cell relaxations, and fitting the resultant energy-volume data to the Murnaghan equation of state. To allow calculation of lithium intercalation energies, reference calculations with the appropriate functionals were performed for a Li_2 cell using the same convergence criteria as above and with a $16 \times 16 \times 16$ Monkhorst-Pack grid for k-point sampling. For stoichiometric TiO_2(B), and one x(Li) = 0.25 Li-TiO_2(B) configuration, we also performed calculations using the HSE06 hybrid density functional, in which a percentage of the exact nonlocal Fock exchange ($\alpha = 0.25$) is introduced to the PBE functional. This typically gives improvements over both LDA and GGA calculations in predicting physical properties such as cell shape,[77] and also has been successful in describing localized polaronic systems.[40,78] The HSE06 calculations were performed with a $1 \times 3 \times 2$ Γ-centered Monkhorst-Pack k-point grid, and all other parameters as for the PBE calculations.

When performing calculations that describe localized electrons (or holes) at specific sites, typically there exist a number of competing electronic minima. Polaron formation is associated with strong coupling between electronic localization and local distortions of geometry,[79] and individual calculations can easily become trapped in metastable electronic minima where electronic localization occurs at nonoptimal sites. A full picture of such a system requires an exhaustive enumeration of all possible minima, which can then be considered to give an approximate description of the time-averaged charge distribution.[55,58] This approach is computationally prohibitive when also comparing multiple atomic geometries, as is the case when modeling possible Li distributions. Differences in energies of up to 0.2 eV e^{-1} have been predicted for competing localized electron distributions at the rutile TiO_2 (110) surface, where there are large variations in electrostatic potential.[55,57,58,80] For Li-doped bulk systems, however, smaller energy differences have been predicted: for example, in Li-anatase TiO_2, the energy difference between an electron localized at a favored Ti site neighboring the

TABLE I. Experimental and calculated structural parameters for stoichoimetric TiO_2(B). For the calculated values, percentage errors relative to the experimental neutron data are given in brackets (Ref. 81). [PW] denotes calculations performed using a plane-wave basis set, and [GTO] and [PAO] denote a basis of atomic orbitals (Gaussian and pseudoatomic, respectively) (Refs. 13 and 82). The PW91 plane-wave basis calculations of Arrouvel *et al*. were constrained to experimental cell shape [PW-c] (Ref. 12). (The volume differences relative to experiment given in the Supplemental Material in the paper of Arrouvel *et al*. are incorrect by a factor of 2.)

Functional	V	a	b	c	β
Neutrons (Ref. 81)	284.22	12.1787	3.7412	6.5249	107.054
XRD (Ref. 82)	285.9	12.197 (8)	3.7537	6.535	107.17
LDA	281.11 (−1.1)	12.1381 (−0.3)	3.7311 (−0.3)	6.4871 (−0.6)	106.894
PW91	295.33 (+3.9)	12.3229 (+1.2)	3.7823 (+1.1)	6.6240 (+1.5)	106.950
PBE	296.03 (+4.2)	12.3277 (+1.2)	3.7857 (+1.2)	6.6298 (+1.6)	106.903
PBEsol	288.59 (+1.5)	12.2363 (+0.5)	3.7647 (+0.6)	6.5473 (+0.3)	106.895
PBE + U	309.47 (+8.9)	12.5441 (+3.0)	3.8909 (+4.0)	6.6314 (+1.6)	107.031
PBEsol + U	302.33 (+6.4)	12.4513 (+2.2)	3.8671 (+3.4)	6.5649 (+0.6)	106.981
HSE06	288.70 (+1.6)	12.2408 (+0.5)	3.7679 (+0.7)	6.5442 (+0.4)	106.964
PBE [PW] (Ref. 82)	293.00 (+3.4)	12.310 (+1.1)	3.764 (+0.6)	6.635 (+1.7)	107.0
PBE [GTO] (Ref. 82)	293.65 (+3.3)	12.3013 (+1.1)	3.7576 (+0.4)	6.6361 (+1.7)	106.8
B3LYP [GTO] (Ref. 82)	291.86 (+2.7)	12.2796 (+0.8)	3.7475 (+0.2)	6.6243 (+1.5)	106.78
PW91 [PW-c] (Ref. 12)	291.91 (+2.7)	12.2875 (+0.9)	3.7746 (+0.9)	6.5832 (+0.9)	107.054
PBE [PAO] (Ref. 13)	293.05 (+3.1)	12.2512 (+0.6)	3.7904 (+1.3)	6.6015 (+1.2)	107.068
PBE [PW] (Ref. 84)	292.54 (+2.9)	12.297 (+1.0)	3.755 (+3.7)	6.625 (+1.5)	107.0

interstitial ion, and for a completely separated Li-e$^-$ pair is calculated to be 56 meV.[36] For the GGA + U calculations described here, a number of optimizations from different starting geometries have been considered for each configuration, with the lowest-energy solution reported. While this is by no means exhaustive, all our GGA + U solutions show the same qualitative behavior, as detailed in the following, suggesting that this general description is not sensitive to the precise distribution of localized electrons or lithium ions.

III. RESULTS

A. Stoichiometric TiO_2(B)

We first consider the accuracy of each selected functional in reproducing the experimental cell dimensions for stoichiometric TiO_2(B). Table I compares calculated structural parameters with those from experimental neutron and x-ray data,[81,82] and from previous calculations.[10,12,13,82–84]

LDA underestimates the lattice parameters and cell volume (−1.1%), and GGA (PBE/PW91) calculations give an overestimation of lattice parameters and cell volume (+3%–4%), as is typical for these functionals. The lattice parameter errors for both LDA and GGA (PBE/PW91) are larger for c than the a or b axes, showing how fully relaxed calculations give small errors in both the shape and volume of the TiO_2(B) unit cell. PBEsol offers improvement over the PW91/PBE GGA functionals, with volume and lattice parameter errors reduced by more than 50%, and this functional can therefore be expected to give improvements in results that are sensitive to errors in cell dimensions, as suggested by Arrouvel *et al*. to be the case for lithium site preference.[12] In particular, the c parameter error is reduced from +1.6% to +0.3% between PBE and PBEsol. Interestingly, PBEsol gives comparable cell-dimension accuracy to the more computationally expensive hybrid HSE06 functional, although this latter calculation is expected to be less accurate due to the reduced density of the corresponding k-point mesh. The PBE + U and PBEsol + U calculations both give much greater volume and lattice parameter overestimations than the equivalent PBE/PBEsol functionals. This is a common consequence of such +U calculations. Although the Ti d states to which this correction is applied are formally unoccupied in the stoichiometric system, the +U term drives a rehybridization of the O $2p$ dominated valence band, which reduces the mixing with Ti $3d$ states and produces an increase in cell volume and band gap.

B. Dilute limit [x(Li) ≈ 0.02]

To represent the dilute limit of Li intercalation into TiO_2(B), we considered a single Li atom at an A1, A2, or C site in a $1 \times 3 \times 2$ supercell, corresponding to x(Li) ≈ 0.02. This is the same supercell expansion used by Panduwinata and Gale, and allows for a direct comparison between our PBE data and these previous results.[13] At these low-Li concentrations, the lattice strain due to the intercalated lithium is expected to be minimal, and stoichiometric cell parameters were used. This assumption was tested by performing full cell relaxations (zero pressure) for the PBE configurations, which gave a maximum change in site energies of 17 meV for A1, which is much smaller than the difference in energies between {C,A2} and A1, as described below. The relative energies for lithium occupation of the A1, A2, and C sites for each functional are shown in Fig. 2, along with the PBE data from Panduwinata and Gale.[13] These site energies vary as [E(A2) ≈ E(C) < E(A1)], with E(C) slightly higher than E(A2) for all functionals apart from PBEsol. These results in general agree with those of Panduwinata and Gale who found for this composition [E(A2) < E(C) < E(A1)], albeit with a larger energy difference of >0.1 eV between the A2 and C sites.[13] This

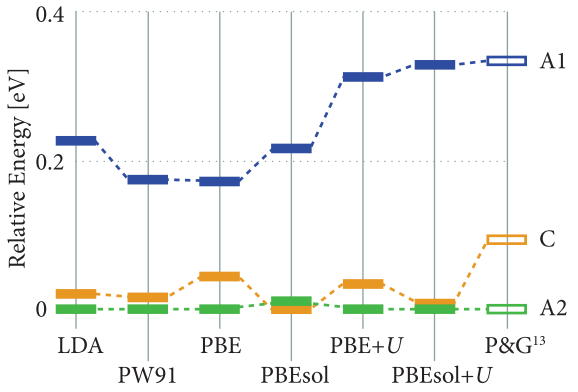

FIG. 2. (Color online) Relative energies of Li sites at $x(\mathrm{Li}) \sim 0.02$ for the considered functionals. The PBE data of Panduwinata and Gale at this composition are included for comparison (open symbols) (Ref. 13).

difference may be due to the choice of pseudoatomic orbitals as the basis set in this previous work, versus a plane-wave basis for the calculations described here. No qualitative difference is found for the GGA versus GGA + U calculations, but the GGA + U results give a slightly larger energy difference between the A1 and A2/C site occupations.

Figure 3 shows the calculated electronic density of states (EDOS) for lithium at the A1, A2, and C sites for the PBE and PBE + U calculations. With PBE, the excess charge density introduced upon lithium intercalation occupies the bottom of the conduction band, giving a metallic system. The projected charge densities associated with these occupied conduction band states are delocalized over all the Ti sites in the calculation [Figs. 3(a)–3(c)]. This delocalization behavior is typical when using standard LDA/GGA density functionals to model n-type defects in TiO_2 where the excess charge is donated to the Ti sublattice.[31,36,62] LDA, PW91, and PBEsol calculations similarly predict delocalized occupied states at the bottom of the conduction band. The excess charge associated with these defect states is now strongly localized at a single Ti site neighboring the interstitial Li. With PBE + U, the density of states shows a defect state in the band gap, approximately 1.5 eV from the bottom of the conduction band. The splitting between occupied and unoccupied Ti d states is larger for these TiO_2(B) calculations than was predicted for lithium intercalated into anatase TiO_2 with the same calculation parameters.[36] This greater splitting of Ti d states suggests that electrons may trap as polarons more strongly in TiO_2(B) than in anatase TiO_2.

C. $x(\mathrm{Li}) = 0.125$

In addition to modeling the dilute limit, we have also considered compositions of $x(\mathrm{Li}) = 0.125$ and 0.25. At these Li concentrations, the TiO_2(B) cell is expected to respond strongly to the intercalated lithium, with experiment showing a highly anisotropic 6.1% volume expansion for $x(\mathrm{Li}) = 0.25$,[10,12] requiring that these calculations be performed with full optimizations of cell shape and volume. A composition of $x(\mathrm{Li}) = 0.125$ is equivalent to one lithium ion per TiO_2(B) unit cell, and for each functional we performed calculations with lithium at each of the three potential sites.

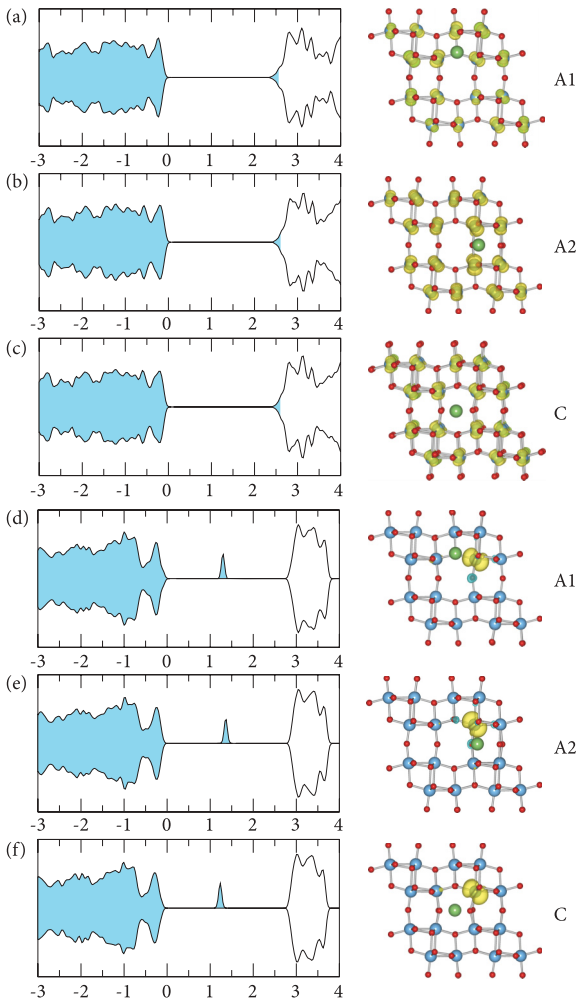

FIG. 3. (Color online) (Left panels) Electronic densities of states for the PBE and PBE + U calculations of a single lithium in a 1 × 3 × 2 supercell at the A1, A2, and C interstitial sites. For each calculation, the energy scale is zeroed at the top of the valence band, and the shading indicates occupied states. (Right panels) Charge densities associated with the excess charge in each calculation. For the PBE calculations, this corresponds to the occupied states at the bottom of the conduction band and for the PBE + U calculations to the defect states in the band gap. Isosurfaces are shown at 0.0035 eV $\mathrm{Å}^{-3}$ for (a)–(c) and 0.05 eV $\mathrm{Å}^{-3}$ for (d)–(f).

These calculations may not be assumed to be representative of experimental samples at this stoichiometry since it is thought that below $x(\mathrm{Li}) = 0.25$, lithitated TiO_2(B) samples exist as a phase-separated mixture of dilute TiO_2(B) and $Li_{0.25}TiO_2$(B) regimes.[10] These calculations, however, allow for a direct comparison with those of Arrouvel *et al.* and Dalton *et al.* and also provide a fuller picture of the variation in site energies with lithium concentrations and across functionals.

The relative energies of lithium occupation of each of the three sites across the considered functionals are compared in Fig. 4, along with the data of Arrouvel *et al.* and Dalton *et al.*[12,14] Every functional gives A2 as the most stable site for lithium accommodation, repeating the result found for the dilute limit. At that lower concentration, however, the C

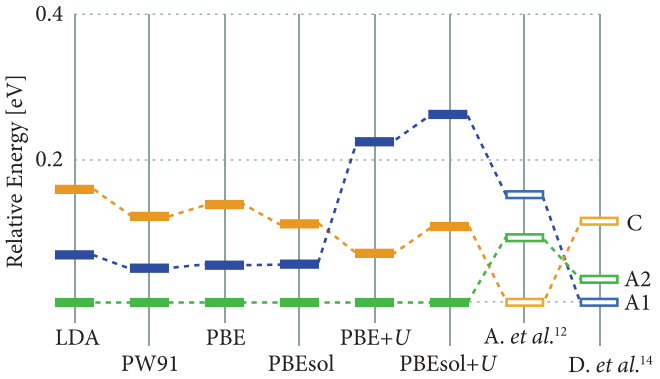

FIG. 4. (Color online) Relative energies of Li sites at $x(\mathrm{Li}) = 0.125$. The PW91 data of Arrouvel *et al*. and PBE data of Dalton *et al*. are included for comparison (open symbols) (Refs. 12 and 14).

site was competitive with A2. In contrast, here the C site is 0.1–0.17 eV less favored than the A2 site. For the LDA/GGA calculations, this places the C site above both A2 and A1 to give relative site energies of $[E(\mathrm{A2}) < E(\mathrm{A1}) < E(\mathrm{C})]$. This contradicts the PW91 results of Arrouvel *et al*. who reported relative site energies of $[E(\mathrm{C}) < E(\mathrm{A2}) < E(\mathrm{A1})]$, and the PBE results of Dalton *et al*. who reported relative site energies of $[E(\mathrm{A1}) < E(\mathrm{A2}) < E(\mathrm{C})]$. Both GGA + U functionals give a small lowering in relative energy of the C site, and an increase in relative energy of the A1 site, making the relative site energies $[E(\mathrm{A2}) < E(\mathrm{C}) < E(\mathrm{A1})]$. The effect of the $+U$ correction is explored in Fig. 5, which shows the relative site energies for PBE + U calculations for $U = 0 \rightarrow 7$ eV. With increasing U, the A1 site energy increases relative to both A2 and C. Between $U = 0$ eV and $U \approx 3$ eV, there is also a small reduction in the relative energy of A2 and C, which stabilizes for $U > 3$ eV. $U = 3$ eV is the point at which the approximate self-interaction correction provided by the $+U$ term "switches on" and it becomes favorable to localize the excess charge at single Ti centres rather than delocalize over all available atoms.[31]

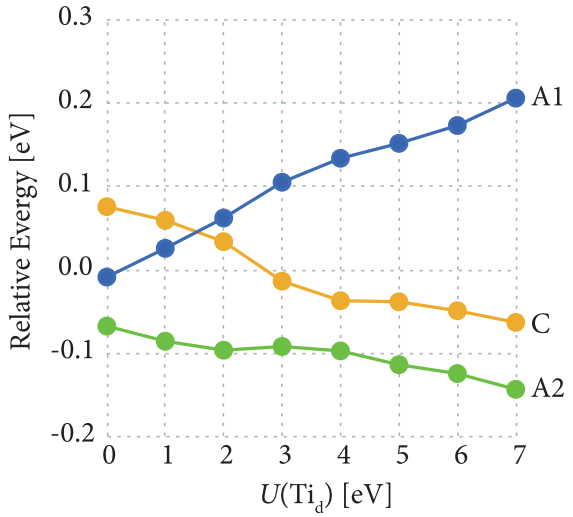

FIG. 5. (Color online) Relative energy of lithium occupation of the A1, A2, and C sites at $x(\mathrm{Li}) = 0.125$ calculated with PBE + U as a function of the U parameter.

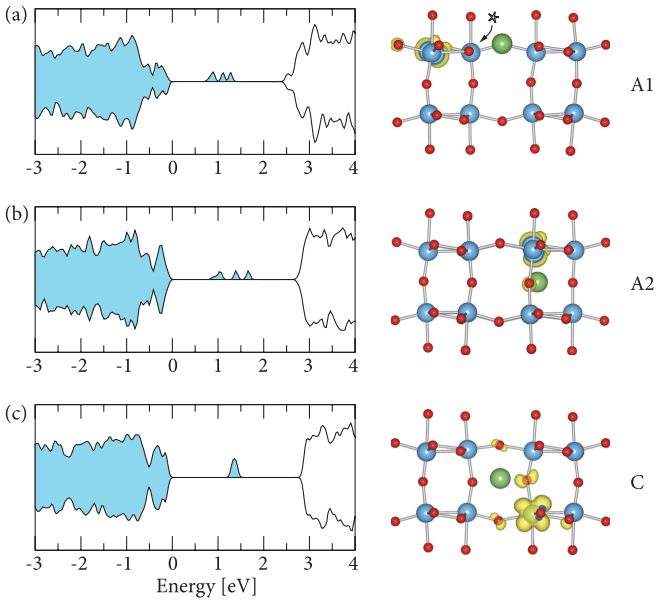

FIG. 6. (Color online) (Left panels) Electronic densities of states for the A1-, A2-, and C-site occupations at $x(\mathrm{Li}) = 0.125$ with PBE + U. For each calculation, the energy scale is zeroed at the top of the valence band, and the shading indicates occupied states. (Right panels) Charge densities corresponding to the defect states in the band gap for each configuration. Isosurfaces are shown at 0.05 eV Å^{-3}. In (a), ⋆ indicates the Ti site adjacent to the Li discussed in the text.

The electronic structures obtained at $x(\mathrm{Li}) = 0.125$ are similar to those at $x(\mathrm{Li}) = 0.02$. The LDA/GGA functionals predict metallic systems where the excess charge occupies the bottom of the conduction band, and is delocalized over all the Ti sites in the calculations. In contrast, the PBE + U calculations predict defect states in the band gap that correspond to strongly localized polaronic states at single Ti sites [Figs. 6(a)–6(c)]. In the dilute limit, the electronic densities of states for the A1, A2, and C PBE + U calculations were quite similar, with the gap states appearing as narrow peaks [Figs. 3(d)–3(f)]. At $x(\mathrm{Li}) = 0.125$, there are now appreciable differences between the three calculation sites. For C-site occupation, the defect peak is narrow, whereas for A1 and A2, the peaks appear split due to dispersion of these states in k space. The degree of dispersion for each defect state is associated with the orientation of the corresponding occupied Ti 3d orbital. These calculations are single TiO_2(B) unit cells, which have their narrowest dimension along b. Since the calculations are periodic, occupied Ti 3d orbitals can be expected to interact with their periodic images along ⟨010⟩. Along ⟨100⟩ and ⟨001⟩, the occupied Ti orbitals are separated and not expected to directly interact. The site preference for the trapped electron and the orientation of the occupied orbital now vary between Li sites, with this presumably a consequence of factors including direct Li-Ti^{3+} interactions, and the differences in cell shape due to the differing locations of the intercalated Li, and the resultant lattice strain. For the C-site calculation, the occupied Ti 3d orbital is oriented in the (010) plane, explaining the absence of any strong interactions along ⟨010⟩ that might otherwise give rise to dispersion in k space.

For the A1 and A2 cases, however, the occupied orbitals lie in the (001) and (100) planes, respectively, with nodes oriented towards those of their periodic images. From electrostatic considerations, it might be expected that the favored position for localization of the excess electronic charge would be at a Ti site neighboring the interstitial Li^+, and this is indeed seen in the dilute limit here and in the anatase TiO_2 phase.[36] Interestingly, for the A1 configuration at $x(\mathrm{Li}) = 0.125$, the electron localizes preferentially at a next-nearest neighbor Ti site from the interstitial position, with localization at an alternative neighboring site (indicated in Fig. 6) 22 meV higher in energy.

1. *Effect of volume on Li site preference*

The energy for intercalation at each of the A1, A2, and C sites is in part determined by the size of the available space and the ability of the lattice to accommodate any strain resulting from incorporation of a lithium ion. Both of these factors will be modified by changes in lattice volume: in experimental samples due to external pressure or to strain inherent to specific morphologies, and the anisotropy of the lattice allows this to differ between the three sites, potentially modifying the relative site energies. Arrouvel *et al.* have discussed the relationship between relative site energies and cell volumes, and proposed that this explains their observation that $x(\mathrm{Li}) = 0.125$ PW91 and PW91 + U calculations give different site preferences. They argued that since the C site is larger than either the A1 and A2 sites, increases in cell volume penalize occupation of the C site with respect to the A1 and A2 sites. While the calculations presented here show the A2 site to be preferred for all considered functionals at their respective appropriate zero-pressure lattice parameters, it is interesting to consider the possible effect of changes in volume. This could be of particular importance in nanoscale samples or thin films, where equilibrium lattice parameters may differ from those in the bulk in response to surface tensions or interfacial strain.

Figure 7 shows volume-energy curves for Li at the A1, A2, and C sites at $x(\mathrm{Li}) = 0.125$ calculated with LDA, PBE, and PBE + U, plotted as reduced volumes V/V_0, where V_0 is the minimum energy volume for the most stable Li configuration (A2). All three configurations show minimum energy volumes that increase for LDA < PBE < PBE + U, as expected from the stoichiometric volume data in Table I. While no experimental structural data exist for $x(\mathrm{Li}) = 0.125$, volume errors with respect to experiment at $x(\mathrm{Li}) = 0$ are −1.1% for LDA, +4.2% for PBE, and +8.9% for PBE + U. LDA and PBE give similar results, whereas with PBE + U there is an increase in E(A1) and slight lowering of E(C) relative to E(A2), as seen in Fig. 4. The *relative* positions of the volume-energy minima are approximately unchanged between the data sets. All three configurations have similar minimum energy volumes, with that of C slightly smaller than A1 and A2. The C site energy has a smaller curvature than the A1 and A2 sites, and so for a sufficient reduction in volume (increased pressure) the C site becomes the most stable. Arrouvel *et al.* argued that the C site would *less* stable for functionals with larger equilibrium volumes. In contrast, we find that those functionals that overestimate cell volumes

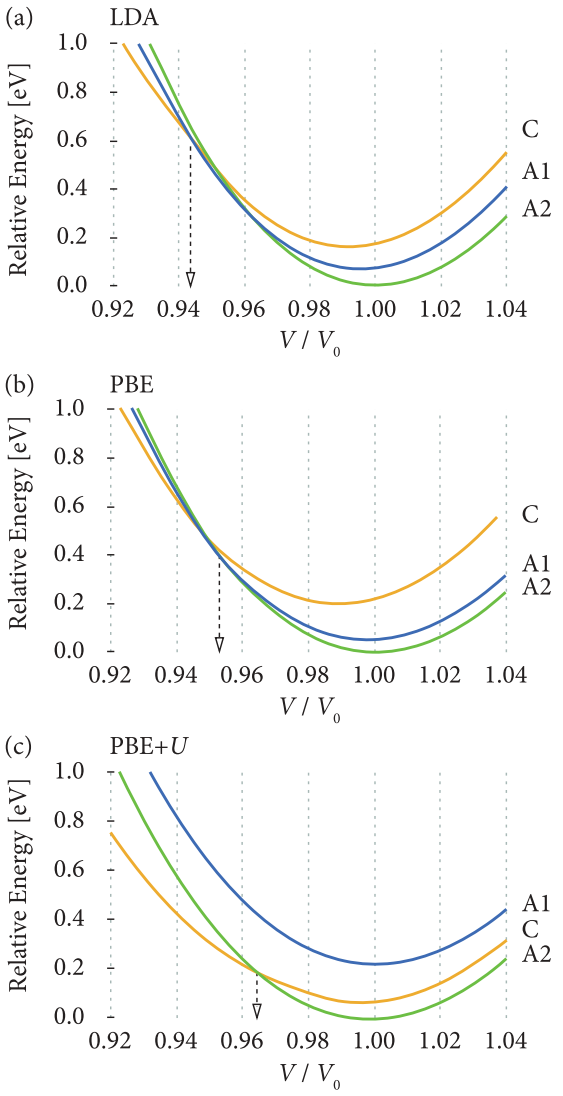

FIG. 7. (Color online) Relative energies as a functional of reduced unit-cell volume V/V_0 for LDA, PBE, and PBE + U at $x(\mathrm{Li}) = 0.125$. The dashed arrows show the reduced volume below which $E(\mathrm{C}) < \{E(\mathrm{A1}), E(\mathrm{A2})\}$.

(PBE/PBE + U) predict a smaller change in volume from the equilibrium values is necessary to stabilize the C site with respect to A1 and A2, while LDA, which underestimates cell volumes, predicts that a greater volume reduction is needed.

D. x(Li) = 0.25

At a lithium concentration of $x(\mathrm{Li}) = 0.25$, two intercalated lithium atoms are accommodated per unit cell of TiO_2(B). The TiO_2(B) unit cell has four A1 sites, four A2 sites, and two C sites available. Considering only symmetry inequivalent arrangements within a single unit cell, and assuming that both lithium ions occupy the same kind of site, there are eight possible arrangements, shown in Fig. 8. For the C sites, the off-center position of the lithium allows two distinct configurations to be considered, depending on whether the displacement along $\pm b$ is symmetric (C_a) or antisymmetric (C_b).[10,12] It is possible that preferred lithium arrangements exist with lower

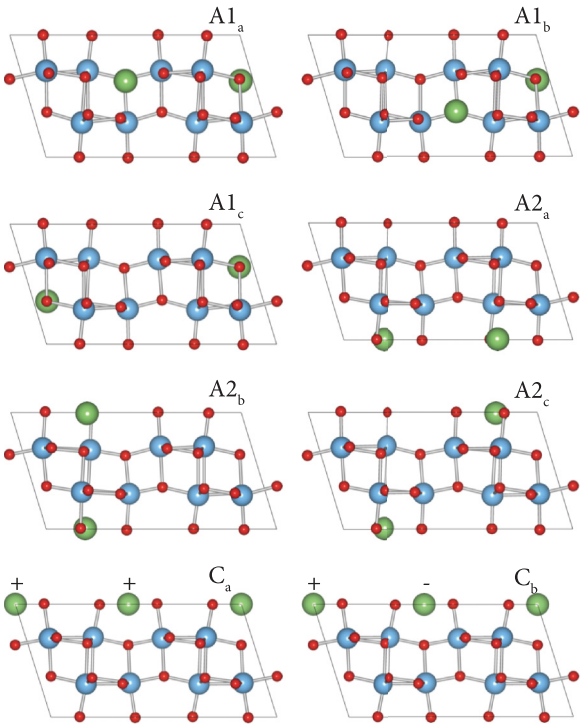

FIG. 8. (Color online) Symmetry inequivalent configurations for a single $Li_{0.25}TiO_2$(B) cell, given that both Li ions adopt the same kind of site. + and − indicate relative displacements of ions into and out of the plane of the figure, respectively.

symmetry than can be accommodated in a single periodic cell, for example a superlattice, as predicted for the orthorhombic TiO_2 phase formed upon lithium intercalation into anatase TiO_2.[85] Modeling all possible configurations for a larger supercell is, however, prohibitively expensive due to the much greater number of inequivalent configurations to be considered and the increased expense of individual calculations, even if considering only those configurations where all the Li occupy the same kind of interstitial site.

The relative energies of the eight considered $x(\mathrm{Li}) = 0.25$ configurations are shown in Fig. 9. The LDA and GGA calculations give the same trends with configuration energies that vary as $[\mathrm{A1_a} < \mathrm{A1_b} < \mathrm{A2_a} \approx \mathrm{A2_c} < \mathrm{A2_b} \approx \mathrm{A1_c} \ll \mathrm{C_b} \approx \mathrm{C_a}]$. The low-energy $\mathrm{A1_a}$ configuration has both Li ions in the same (001) plane, in agreement with the lowest-energy configuration identified by Dalton *et al.*[14] For the GGA + U calculations, the site preference is $[\mathrm{A2_b} < \mathrm{A2_c} < \mathrm{A2_b} < \mathrm{C_a} \approx \mathrm{C_b} \approx \mathrm{A1_a} \ll \mathrm{A1_b} \approx \mathrm{A1_c}]$. Figure 10 shows the variation in relative energies for each configuration for PBE + U for $U = 0 \rightarrow 7$ eV. This is more complex than the equivalent data at $x(\mathrm{Li}) = 0.125$ due to the greater number of configurations, but shows similar behavior: all three A1 configurations become increasingly disfavored with increasing U; the $\mathrm{A1_a}$ and $\mathrm{A1_b}$ configurations favored for $U = 0$ eV become unstable with respect to A2 occupation at small values of U, and the $\mathrm{C_a}$ and $\mathrm{C_b}$ configurations are stabilized. Hence, the general site preference at $U > 4$ eV is the same as for the $x(\mathrm{Li}) = 0.125$ GGA + U calculations: $[E(\mathrm{A2}) < E(\mathrm{C}) < E(\mathrm{A1})]$.

Figure 11 shows the electronic densities of states and excess charge distributions for the $x(\mathrm{Li}) = 0.25$ configurations

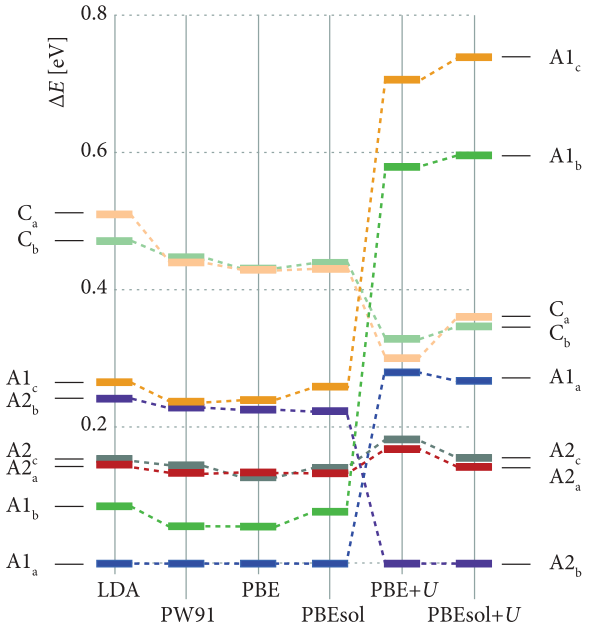

FIG. 9. (Color online) Relative energies of Li sites at $x(\mathrm{Li}) = 0.25$.

obtained with PBE + U. In each case, the lowest-energy spin solution is shown. In contrast to the LDA and GGA calculations, which give delocalized metallic solutions with charge distributed over all the Ti sites, all considered configurations show defect states in the band gap, associated with pairs of electrons strongly localized at two Ti centres. For most configurations, the defect states show splitting associated with dispersion of the associated bands in k space due to

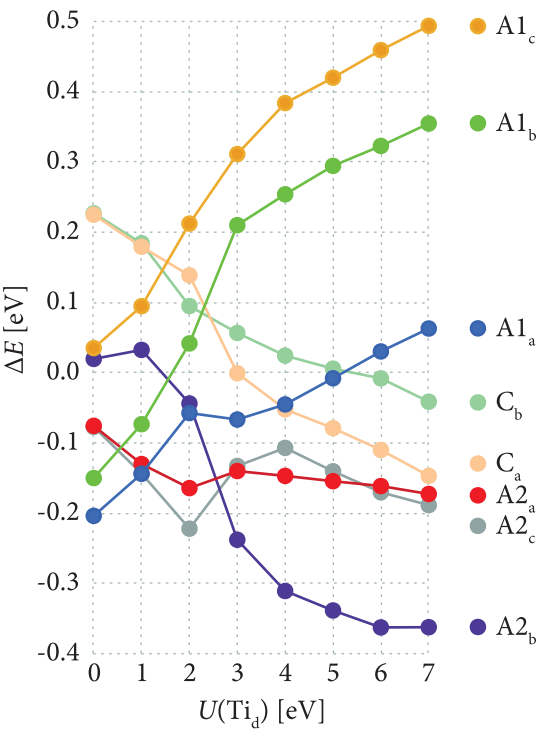

FIG. 10. (Color online) Variation in relative energies with $U(\mathrm{Ti}_d)$ of configurations at $x(\mathrm{Li}) = 0.25$.

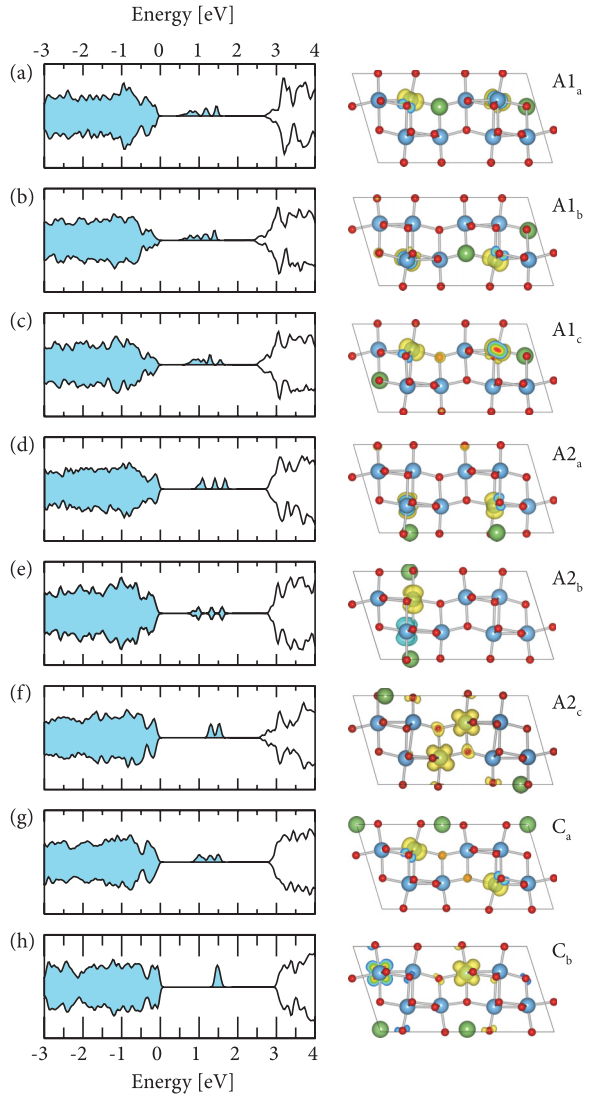

FIG. 11. (Color online) (Left panels) Electronic densities of states for the PBE + U x(Li) = 0.25 configurations. For each calculation, the energy scale is zeroed at the top of the valence band, and the shading indicates occupied states. (Right panels) Charge density associated with the defect states for each configuration. Each charge isosurface is shown at 0.05 eV Å^{-3}.

the interaction of the occupied Ti 3d orbitals with their neighboring periodic images along ⟨010⟩, as seen at x(Li) = 0.125. In contrast, the C_b configuration [Fig. 11(h)] shows a single defect peak in the EDOS, and the associated occupied Ti 3d states are oriented in the (010) plane, with this presumably minimizing the interaction between periodic images along the perpendicular direction, as seen for configuration C at x(Li) = 0.125. The $A2_b$ configuration shows a similar (010) orientation of the occupied Ti 3d orbitals but two defect peaks in band gap of the EDOS, which appears inconsistent with the model of splitting due to band dispersion along the |010| k vector. In this case, the splitting is due to a real-space interaction between the two occupied Ti 3d orbitals, which are located on neighboring sites and form a hybridized bonding-antibonding pair of states.[64] The distribution of localized electrons also plays a role in the energy difference between the spin-paired ($M_s = 0$) and spin-parallel ($M_s = 1$) solutions for each Li configuration. In all calculations where the electrons are localized at non-neighboring Ti sites, the energy difference between spin-paired and spin-parallel solutions is <2 meV. The relative spins of the two localized electrons are only significant for configurations $A2_b$ and $A2_c$ where the electrons are found at neighboring Ti centers. For the $A2_b$ configuration, the spin-paired $M_s = 0$ solution is 18 meV more stable than the equivalent spin-parallel solution, whereas for $A2_c$ the spin-paired solution is 169 meV *less* stable than the equivalent spin-paired solution.

For each lithium configuration, one can propose a number of alternative solutions where the excess electrons are localized at different pairs of Ti sites, and these are expected to be sampled according to a Boltzmann distribution at any nonzero temperature, within the adiabatic approximation.[55,58] To examine the energy scale associated with these alternate configurations, we performed additional calculations for the C_a lithium configuration with each symmetry inequivalent pair of Ti atoms considered as sites to accommodate the two excess electrons. For each calculation, a full geometric relaxation was performed. The resulting solutions therefore correspond to local minima on an adiabatic potential energy surface. Figure 12 shows the energies of these alternate polaron configurations, relative to the lowest-energy C_a solution shown in Fig. 11, all of which predict insulating defect states in the band gap (Fig. 15). These energies all lie within 0.4 eV of the ground state, which is a similar energy range to that reported by Deskins *et al.* for the different arrangements of pairs of localized electrons associated with an oxygen vacancy at the rutile TiO_2 (110) surface.[55] Two configurations, ag and eg, are within 20 meV of the most stable configuration, and another two configurations, dg and cf, have relative energies of only 80 meV, and these are therefore expected to appreciably be sampled at nonzero temperatures. Therefore, the excess electrons should not be thought of as trapped indefinitely at specific sites, but instead for each lithium configuration there

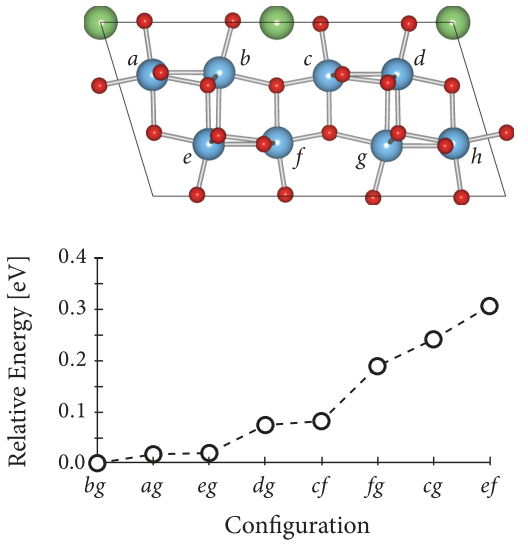

FIG. 12. (Color online) Relative energies of the eight symmetry inequivalent Ti^{3+} configurations for the C_a lithium geometry.

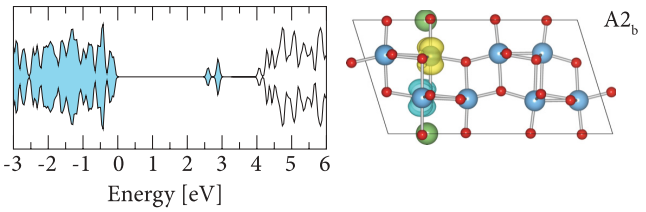

FIG. 13. (Color online) (Left panel) Electronic density of states for the $A2_b$ $x(\mathrm{Li}) = 0.25$ configuration, calculated with the HSE06 hybrid functional. The energy scale is zeroed at the top of the valence band, and the shading indicates occupied states. (Right panel) Charge density associated with the defect states. The charge isosurface is shown at 0.05 eV $\mathrm{Å}^{-3}$.

are multiple nearly degenerate solutions sampled as electrons move between accessible sites.

An additional consideration is that a poor choice of projection operators can bias the calculated electronic structure towards an unphysical charge distribution. Here, our projection operators are atom-centered spherical harmonics, and the $+U$ calculations implicitly assume that the states of interest are well described within such a basis, i.e., are atomiclike. To complement our GGA + U calculations, we performed an additional calculation for the $A2_b$ configuration (the favored configuration from the GGA + U data set) using the HSE06 hybrid density functional, which applies a 25% proportion of screened exact Fock-exchange to all electronic states, without bias towards specific charge distributions.[77] The calculated EDOS and excess charge density distribution are shown in Fig. 13. The excess electronic charge occupies defect states ∼1.2 eV below the conduction-band edge, with a corresponding charge density strongly localized at two Ti sites. The high degree of similarity to the corresponding GGA + U data [Fig. 11(e)] supports the prediction that Li-TiO_2(B) exhibits polaronic trapping of excess electrons corresponding to insulating states in the band gap.

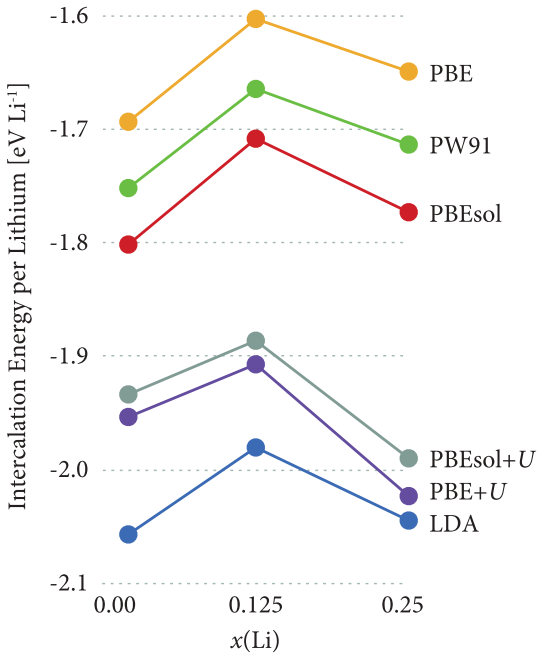

FIG. 14. (Color online) Average intercalation energies for $x(\mathrm{Li}) = 0.02, 0.125, 0.25$ for $\mathrm{Li}_x\mathrm{TiO}_2$(B) for all considered functionals.

E. Intercalation voltages

Intercalation energies per Li (negative average voltages) as a function of x(Li) were calculated as

$$\frac{E(\mathrm{Li}_x\mathrm{TiO}_2) - E(\mathrm{TiO}_2) - xE(\mathrm{Li}_{(s)})}{Fx}, \quad (2)$$

where F is the Faraday constant. These are plotted in Fig. 14 for all considered functionals. All functionals predict that the composition of $x(\mathrm{Li}) = 0.125$ is unstable with respect to phase separation into TiO_2 and $\mathrm{Li}_{0.25}\mathrm{TiO}_2$ domains, in agreement with the neutron data of Armstrong *et al.*[10]

IV. SUMMARY AND DISCUSSION

We have performed DFT calculations of $\mathrm{Li}_x\mathrm{TiO}_2$(B) at $x(\mathrm{Li}) = 0.02, 0.125, 0.25$ with a range of density functionals: LDA, GGA (PW91, PBE, PBEsol), and GGA + U (PBE + U and PBEsol + U). The C site is found to be disfavored with all functionals and at all considered values of x(Li). This challenges the interpretation of previous neutron data, which suggested that the C site is preferentially occupied at $x(\mathrm{Li}) = 0.25$,[10] and with the calculations of Arrouvel *et al.*[12] In the dilute limit, we find that the site energies vary as $[E(\mathrm{A2}) \approx E(\mathrm{C}) < E(\mathrm{A1})]$, with E(C) slightly higher than E(A2) for all functionals apart from PBEsol, in general agreement with the low-x(Li) data of Panduwinata and Gale.[13] At increased lithium concentrations, the A1 and A2 sites are preferred, with differences in the order of relative site energies between the LDA/GGA functionals and the GGA + U calculations. We find at $x(\mathrm{Li}) = 0.125$ relative site energies of $[E(\mathrm{A2}) < E(\mathrm{A1}) < E(\mathrm{C})]$ and $[E(\mathrm{A2}) < E(\mathrm{C}) < E(\mathrm{A1})]$, and at $x(\mathrm{Li}) = 0.25$ relative site energies of $[E(\mathrm{A1}) \approx E(\mathrm{A2}) < E(\mathrm{C})]$ and $[E(\mathrm{A2}) < E(\mathrm{C}) < E(\mathrm{A1})]$, respectively. The change in site preference order between otherwise equivalent GGA and GGA + U calculations shows the assumption of Panduwinata and Gale that energetic trends are not sensitive to the choice of functional to be invalid.[13] The disagreement with the neutron data of Armstrong *et al.* suggests two possibilities: that the preferred lithium site has not been correctly identified from experimental data, or that the Li-rich phases in this low-Li regime do not have a lithium content of precisely $x(\mathrm{Li}) = 0.25$.

In contrast to the suggestion of Arrouvel *et al.*, there is no simple relationship between the volume error expected for a specific functional and the relative energies of the available intercalation sites.[12] Instead, we find that standard functionals give very similar predictions, despite LDA and GGA functionals, respectively, underestimating and overestimating experimental volumes. The GGA + U calculations found a different site ordering, but this is not simply explained by the larger volumes for these functionals, as this might be expected to produce a similar effect for both A1 and A2 sites, which are of similar geometries.

Standard LDA/GGA functionals predict that the excess charge introduced upon lithium intercalation is delocalized over all the Ti sites in the system. This gives a metallic system with the bottom of the conduction band occupied, as seen with these methods for previous studies of Li-intercalated TiO_2 rutile and anatase.[36,85–87] GGA + U calculations instead predict that the excess charge is strongly localized as small polarons as specific Ti sites (formally Ti^{3+}), corresponding to new occupied states in the band gap. Although there currently are no experimental data on the degree of localization and energies of the excess charge states in Li_xTiO_2(B), the simplest expectation is that this polytype behaves in a qualitatively similar fashion to anatase Li-TiO_2, where experimental valence photoemission data indicate excess electron states in the band gap corresponding to localized Ti^{3+} species,[16] in agreement with the +U calculations presented here.

The precise result for a GGA + U calculation depends on the choice of U parameters and projection operators. Optimal +U parameters are structure dependent, and so can be expected to differ between anatase and TiO_2(B). The prediction of *deeper* defect states for the *same* U value, however, may suggest that a small-polaronic description is correct for Li_xTiO_2(B). This interpretation is supported by the qualitatively similar description obtained using the hybrid HSE06 functional for the $A2_b$ configuration at x(Li) = 0.25. Interestingly, even at a lithium content as high as x(Li) = 0.25 where significant interactions are expected between the excess electrons, the occupied defect states do not cross the bottom of the conduction band, and so semiconducting behavior is still predicted for all arrangements of Li^+ and localized electrons considered here.

ACKNOWLEDGMENT

This work was supported by EPSRC Grant No. EP/H003819/1.

APPENDIX

Tables II, III, IV, and V contain numerical data used to construct Figs. 2, 4, 9, and 14, respectively. Figure 15 shows the calculated EDOS and projected excess charge densities of all symmetry inequivalent Ti^{3+} arrangements for the C_a x(Li) = 0.25 configuration.

TABLE II. Relative energies of Li sites at x(Li) ∼ 0.02 for the considered functionals. The PBE data of Panduwinata and Gale at this composition are included for comparison (Ref. 13).

Functional	A1	A2	C
LDA	0.228	0.000	0.021
PW91	0.175	0.000	0.016
PBE	0.173	0.000	0.044
PBEsol	0.217	0.011	0.000
PBE + U	0.314	0.000	0.034
PBEsol + U	0.331	0.000	0.008
P&G (Ref. 13)	0.336	0.000	0.094

TABLE III. Relative energies of Li sites at x(Li) = 0.125. The PW91 data of Arrouvel *et al.* and PBE data of Dalton *et al.* are included for comparison (Refs. 12 and 14).

Functional	A1	A2	C
LDA	0.067	0.000	0.158
PW91	0.048	0.000	0.121
PBE	0.052	0.000	0.137
PBEsol	0.054	0.000	0.110
PBE + U	0.225	0.000	0.069
PBEsol + U	0.262	0.000	0.106
Ref. 12	0.150	0.090	0.000
Ref. 14	0.000	0.032	0.113

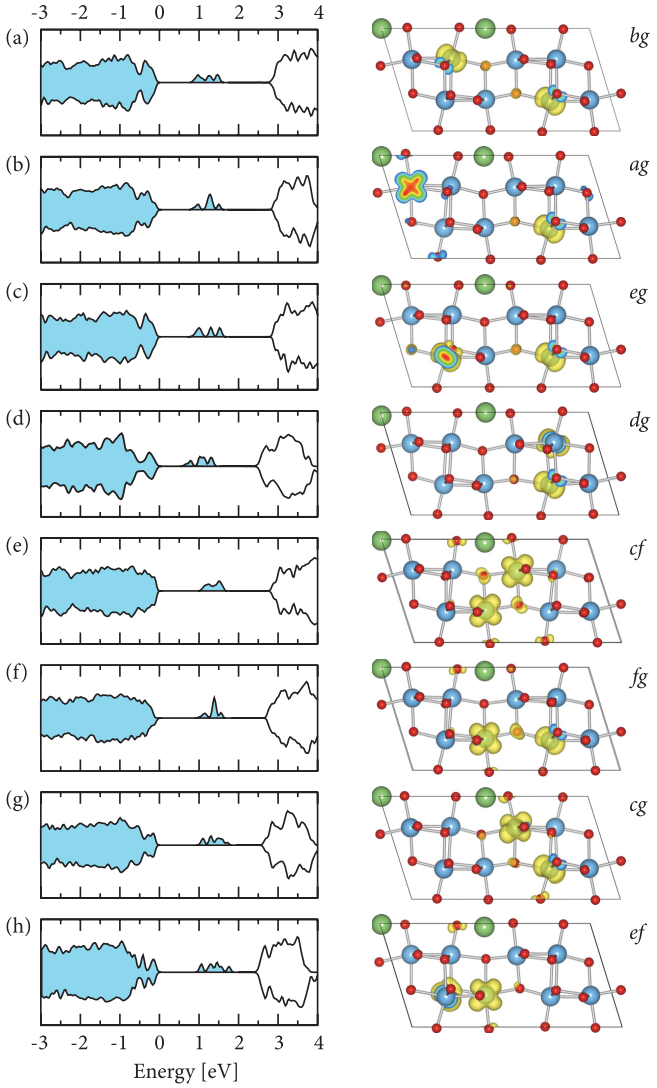

FIG. 15. (Color online) (Left panels) PBE + U electronic densities of states for the x(Li) = 0.25 C_a configuration considering all inequivalent positions for the polaron pairs. For each calculation, the energy scale is zeroed at the top of the valence band, and the shading indicates occupied states. (Right panels) Charge density associated with the defect states for each configuration. Each charge isosurface is shown at 0.05 eV $Å^{-3}$.

TABLE IV. Relative energies of Li sites at $x(\mathrm{Li}) = 0.25$.

Functional	$A1_a$	$A1_b$	$A1_c$	$A2_a$	$A2_b$	$A2_c$	C_a	C_b
LDA	0.000	0.084	0.265	0.145	0.241	0.153	0.510	0.471
PW91	0.000	0.055	0.237	0.133	0.228	0.144	0.440	0.447
PBE	0.000	0.054	0.239	0.133	0.225	0.126	0.429	0.431
PBEsol	0.000	0.076	0.258	0.132	0.223	0.140	0.430	0.439
PBE + U	0.279	0.579	0.707	0.167	0.000	0.061	0.300	0.328
PBEsol + U	0.267	0.596	0.740	0.141	0.000	0.154	0.360	0.346

TABLE V. Intercalation energies as a function of $x(\mathrm{Li})$, calculated according to Eq. (2).

Functional	$x = 0.02$	$x = 0.125$	$x = 0.25$
LDA	−2.06	−1.98	−2.04
PW91	−1.75	−1.66	−1.71
PBE	−1.69	−1.60	−1.65
PBEsol	−1.80	−1.71	−1.77
PBE + U	−1.95	−1.91	−2.02
PBEsol + U	−1.93	−1.89	−1.99

*benjamin.morgan@materials.ox.ac.uk

[1] E. Ferg, J. Gummow, A. de Kock, and M. M. Thackeray, J. Electrochem. Soc. **141**, L147 (1994).

[2] T. Ohzuku, A. Ueda, and N. J. Yamamoto, J. Electrochem. Soc. **142**, 1431 (1995).

[3] M. Zukalová, M. Kalbác, L. Kavan, I. Exnar, and M. Graetzel, Chem. Mater. **17**, 1248 (2005).

[4] J. B. Goodenough and Y. Kim, Chem. Mater. **22**, 587 (2010).

[5] R. Marchand, L. Brohan, and M. Tournoux, Mater. Res. Bull. **15**, 1129 (1980).

[6] R. J. Cava, D. W. Murphy, S. Zahurak, A. Santoro, and R. S. Roth, J. Solid State Chem. **53**, 64 (1984).

[7] A. R. Armstrong, G. Armstrong, J. Canales, R. Garcia, and P. G. Bruce, Adv. Mater. **17**, 862 (2005).

[8] A. R. Armstrong, G. Armstrong, J. Canales, and P. G. Bruce, Angew. Chem. Int. Ed. **43**, 2286 (2004).

[9] G. Armstrong, A. R. Armstrong, J. Canales, and P. G. Bruce, Chem. Commun. 2454 (2005).

[10] A. R. Armstrong, C. Arrouvel, V. Gentili, S. C. Parker, M. S. Islam, and P. G. Bruce, Chem. Mater. **22**, 6426 (2010).

[11] L. Brohan and R. Marchand, Solid State Ionics **9–10**, 419 (1983).

[12] C. Arrouvel, S. C. Parker, and M. S. Islam, Chem. Mater. **21**, 4778 (2009).

[13] D. Panduwinata and J. D. Gale, J. Mater. Chem. **19**, 3931 (2009).

[14] A. S. Dalton, A. A. Belak, and A. Van der Ven, Chem. Mater. **24**, 1568 (2012).

[15] M. V. Koudriachova, Surf. Interface Anal. **42**, 1330 (2010).

[16] J. H. Richter, A. Henningsson, B. Sanyal, P. G. Karlsson, M. P. Andersson, P. Uvdal, H. Siegbahn, O. Eriksson, and A. Sandell, Phys. Rev. B **71**, 235419 (2005).

[17] A. Henningsson, H. Rensmo, A. Sandell, and H. Siegbahn, J. Chem. Phys. **118**, 5607 (2003).

[18] S. Södergren, H. Siegbahn, H. Rensmo, H. Lindström, A. Hagfeldt, and S.-E. Lindquist, J. Phys. Chem. B **101**, 3087 (1997).

[19] A. Augustsson, A. Henningsson, S. N. Butorin, H. Siegbahn, J. Nordgren, and J.-H. Guo, J. Chem. Phys. **119**, 3983 (2003).

[20] V. E. Henrich, G. Dresselhaus, and H. J. Zeiger, Phys. Rev. Lett. **36**, 1335 (1976).

[21] R. L. Kurtz, R. Stockbauer, and T. E. Madey, Surf. Sci. **218**, 178 (1989).

[22] D. Morris, Y. Dou, J. Rebane, C. E. J. Mitchell, R. G. Egdell, D. S. L. Law, A. Vittadini, and M. Casarin, Phys. Rev. B **61**, 13445 (2000).

[23] S. Yang, L. E. Halliburton, A. Manivannan, P. H. Bunton, D. B. Baker, M. Klemm, S. Horn, and A. Fujishima, Appl. Phys. Lett. **94**, 162114 (2009).

[24] S. Zhou, A. Čižmar, K. Potzger, M. Krause, G. Talut, M. Helm, J. Fassbender, S. A. Zvyagin, J. Wosnitza, and H. Schmidt, Phys. Rev. B **79**, 113201 (2009).

[25] S. Yang and L. Halliburton, Phys. Rev. B **81**, 035204 (2010).

[26] Y. Furubayashi, T. Hitosugi, Y. Yamamoto, K. Inaba, G. Kinoda, Y. Hirose, T. Shimada, and T. Hasegawa, Appl. Phys. Lett. **86**, 252101 (2005).

[27] P. Deák, B. Aradi, and T. Frauenheim, Phys. Rev. B **83**, 155207 (2011).

[28] S. Livraghi, M. Chiesa, M. C. Paganini, and E. Giamello, J. Phys. Chem. C **115**, 25413 (2011).

[29] T. Yamamoto and T. Ohno, Phys. Rev. B **85**, 033104 (2012).

[30] C. Di Valentin, G. Pacchioni, and A. Selloni, Phys. Rev. Lett. **97**, 166803 (2006).

[31] B. J. Morgan and G. W. Watson, Surf. Sci. **601**, 5034 (2007).

[32] C. J. Calzado, N. C. Hernández, and J. F. Sanz, Phys. Rev. B **77**, 045118 (2008).

[33] E. Finazzi, C. Di Valentin, G. Pacchioni, and A. Selloni, J. Chem. Phys. **129**, 154113 (2008).

[34] B. J. Morgan, D. O. Scanlon, and G. W. Watson, J. Mater. Chem. **19**, 5175 (2009).

[35] C. Di Valentin, G. Pacchioni, and A. Selloni, J. Phys. Chem. C **113**, 20543 (2009).

[36] B. J. Morgan and G. W. Watson, Phys. Rev. B **82**, 144119 (2010).

[37] J. P. Perdew and A. Zunger, Phys. Rev B **23**, 5048 (1981).

[38] P. Mori-Sánchez, A. J. Cohen, and W. Yang, Phys. Rev. Lett. **100**, 146401 (2008).

[39] S. Lany and A. Zunger, Phys. Rev. B **80**, 085202 (2009).

[40] D. O. Scanlon, B. J. Morgan, G. W. Watson, and A. Walsh, Phys. Rev. Lett. **103**, 096405 (2009).

[41] K. P. McKenna and A. L. Shluger, Proc. R. Soc. A **467**, 2043 (2011).

[42] S. Lany, Phys. Status Solidi B **248**, 1052 (2011).

[43] W. R. L. Lambrecht, Phys. Status Solidi B **248**, 1547 (2011).

[44] S. J. Clark, J. Robertson, S. Lany, and A. Zunger, Phys. Rev. B **81**, 115311 (2010).

[45] K. G. Godinho, J. Carey, B. J. Morgan, D. O. Scanlon, and G. W. Watson, J. Mater Chem. **20**, 1086 (2010).

[46] S. Lany and A. Zunger, Phys. Rev. B **81**, 205209 (2010).

[47] M. H. Du and S. B. Zhang, Phys. Rev. B **80**, 115217 (2009).

[48] M. Nolan and G. W. Watson, J. Chem. Phys. **125**, 144701 (2006).

[49]D. O. Scanlon, A. Walsh, B. J. Morgan, and G. W. Watson, J. Phys. Chem. C **112**, 9903 (2008).
[50]M. Nolan, S. C. Parker, and G. W. Watson, Phys. Chem. Chem. Phys. **8**, 216 (2006).
[51]R. Coquet and D. J. Willock, Phys. Chem. Chem. Phys. **7**, 3819 (2005).
[52]S. L. Dudarev, G. A. Botton, S. Y. Savrasov, C. J. Humphreys, and A. P. Sutton, Phys. Rev. B **57**, 1505 (1998).
[53]S. L. Dudarev, A. I. Liechtenstein, M. R. Castell, G. A. D. Briggs, and A. P. Sutton, Phys. Rev. B **56**, 4900 (1997).
[54]J. Stausholm-Moller, H. H. Kristoffersen, B. Hinnemann, G. K. H. Madsen, and B. Hammer, J. Chem. Phys. **133**, 144708 (2010).
[55]N. A. Deskins, R. Rousseau, and M. Dupuis, J. Phys. Chem. C **115**, 7562 (2011).
[56]N. A. Deskins, R. Rousseau, and M. Dupuis, J. Phys. Chem. C **114**, 5891 (2010).
[57]N. A. Deskins and M. Dupuis, Phys. Rev. B **75**, 195212 (2007).
[58]N. A. Deskins, R. Rousseau, and M. Dupuis, J. Phys. Chem. C **113**, 14583 (2009).
[59]A. Droghetti, C. D. Pemmaraju, and S. Sanvito, Phys. Rev. B **81**, 092403 (2010).
[60]A. B. Kehoe, D. O. Scanlon, and G. W. Watson, Chem. Mater. **23**, 4464 (2011).
[61]B. J. Morgan and G. W. Watson, Phys. Rev. B **80**, 233102 (2009).
[62]B. J. Morgan, D. O. Scanlon, and G. W. Watson, J. Surf. Sci. Nanotechnol. **7**, 389 (2009).
[63]B. J. Morgan and G. W. Watson, J. Phys. Chem. C **114**, 2321 (2010).
[64]B. J. Morgan and G. W. Watson, J. Phys. Chem. C **113**, 7322 (2009).
[65]C. Di Valentin and A. Selloni, J. Phys. Chem. Lett. **2**, 2223 (2011).
[66]A. Walsh, Y. Yan, M. M. Al-Jassim, and S. H. Wei, J. Phys. Chem. C **125**, 12044 (2008).
[67]S. Chrétien and H. Metiu, J. Phys. Chem. C **115**, 4696 (2011).
[68]F. Zhou, M. Cococcioni, C. A. Marianetti, D. Morgan, and G. Ceder, Phys. Rev. B **70**, 235121 (2004).
[69]J. Perdew, A. Ruzsinszky, G. Csonka, O. Vydrov, G. Scuseria, L. Constantin, X. Zhou, and K. Burke, Phys. Rev. Lett. **100**, 136406 (2008).
[70]G. Kresse and J. Hafner, Phys. Rev. B **49**, 14251 (1994).
[71]G. Kresse and J. Furthmüller, Phys. Rev. B **54**, 11169 (1996).
[72]P. E. Blöchl, Phys. Rev. B **50**, 17953 (1994).
[73]G. Kresse and D. Joubert, Phys. Rev. B **59**, 1758 (1999).
[74]D. Ceperley and B. J. Alder, Phys. Rev Lett. **45**, 566 (1980).
[75]J. P. Perdew and Y. Wang, Phys. Rev. B **45**, 13244 (1992).
[76]J. P. Perdew, R. G. Parr, M. Levy, and B. J. Balduz Jr., Phys. Rev. Lett. **49**, 1691 (1982).
[77]J. Heyd, G. E. Scuseria, and M. Ernzerhof, J. Chem. Phys. **118**, 8207 (2003).
[78]M. V. Ganduglia-Pirovano, J. L. F. Da Silva, and J. Sauer, Phys. Rev. Lett. **102**, 026101 (2009).
[79]A. M. Stoneham, J. Gavartin, A. L. Shluger, A. V. Kimmel, D. M. Ramo, H. M. Ronnow, G. Aeppli, and C. Renner, J. Phys.: Condens. Matter **19**, 255208 (2007).
[80]P. M. Kowalski, M. F. Camellone, N. N. Nair, B. Meyer, and D. Marx, Phys. Rev. Lett. **105**, 146405 (2010).
[81]T. P. Feist and P. K. Davies, J. Solid State Chem. **101**, 275 (1992).
[82]M. Ben Yahia, F. Lemoigno, T. Beuvier, J.-S. Filhol, M. Richard-Plouet, L. Brohan, and M.-L. Doublet, J. Chem. Phys. **130**, 204501 (2009).
[83]A. Vittadini, M. Casarin, and A. Selloni, J. Mater. Chem. **20**, 5871 (2010).
[84]A. Vittadini, M. Casarin, and A. Selloni, J. Phys. Chem. C **113**, 18973 (2009).
[85]B. J. Morgan and G. W. Watson, J. Phys. Chem. Lett. **2**, 1657 (2011).
[86]M. V. Koudriachova, N. M. Harrison, and S. W. de Leeuw, Solid State Ionics **175**, 829 (2004).
[87]M. V. Koudriachova, S. W. de Leeuw, and N. M. Harrison, Phys. Rev. B **69**, 054106 (2004).